Articles

Intercalation of Aflatoxin B_1 in Two Oligodeoxynucleotide Adducts: Comparative ^1H NMR Analysis of d(ATC^{AFB}GAT)·d(ATCGAT) and d(AT^{AFB}GCAT)$_2$†

S. Gopalakrishnan, Thomas M. Harris,* and Michael P. Stone*

Department of Chemistry and Center in Molecular Toxicology, Vanderbilt University, Nashville, Tennessee 37235

Received May 9, 1990; Revised Manuscript Received August 2, 1990

ABSTRACT: 8,9-Dihydro-8-{*N*7-guanyl-[d(ATCGAT)]}-9-hydroxyaflatoxin B_1·d(ATCGAT) and 8,9-dihydro-8-{*N*7-guanyl-[d(ATGCAT)]}-9-hydroxyaflatoxin B_1·8,9-dihydro-8-{*N*7-guanyl-[d(ATGCAT)]}-9-hydroxyaflatoxin B_1 were prepared by direct addition of aflatoxin B_1 8,9-epoxide to d(ATCGAT)$_2$ and d(ATGCAT)$_2$, respectively. In contrast to reaction of aflatoxin B_1 8,9-epoxide with d(ATCGAT)$_2$ which exhibits a limiting stoichiometry of 1:1 aflatoxin B_1:d(ATCGAT)$_2$ [Gopalakrishnan, S., Stone, M. P., & Harris, T. M. (1989) *J. Am. Chem. Soc. 111*, 7232–7239], reaction of aflatoxin B_1 8,9-epoxide with d(ATGCAT)$_2$ exhibits a limiting stoichiometry of 2:1 aflatoxin B_1:d(ATGCAT)$_2$. ^1H NOE experiments, nonselective ^1H T_1 relaxation measurements, and ^1H chemical shift perturbations demonstrate that in both modified oligodeoxynucleotides the aflatoxin moiety is intercalated above the 5′-face of the modified guanine. The oligodeoxynucleotides remain right-handed, and perturbation of the B-DNA structure is localized adjacent to the adducted guanine. Aflatoxin–oligodeoxynucleotide ^1H NOEs are observed between aflatoxin and the 5′-neighbor base pair and include both the major groove and the minor groove. The aflatoxin methoxy and cyclopentenone ring protons face into the minor groove; the furofuran ring protons face into the major groove. No NOE is observed between the imino proton of the modified base pair and the imino proton of the 5′-neighbor base pair; sequential NOEs between nucleotide base and deoxyribose protons are interrupted in both oligodeoxynucleotide strands on the 5′-side of the modified guanine. The protons at C8 and C9 of the aflatoxin terminal furan ring exhibit slower spin–lattice relaxation as compared to other oligodeoxynucleotide protons, which supports the conclusion that they face into the major groove. Increased shielding is observed for aflatoxin protons; chemical shift perturbations of the oligodeoxynucleotide protons are confined to the immediate vicinity of the adducted base pair. The imidazole proton of the modified guanine exchanges with water and is observed at 9.75 ppm. The difference in reaction stoichiometry is consistent with an intercalated transition-state complex between aflatoxin B_1 8,9-epoxide and B-DNA. Insertion of aflatoxin B_1-8,9 epoxide above the 5′-face of guanine in d(ATCGAT)$_2$ would prevent the binding of a second molecule of aflatoxin B_1 8,9-epoxide. In contrast, two intercalation sites would be available with d(ATGCAT)$_2$. Intercalation provides excellent positioning for nucleophilic attack by guanine N7 on aflatoxin B_1 8,9-epoxide, which probably accounts for the observed efficiency of adduct formation despite the relatively low DNA binding affinity observed for aflatoxin B_1.

Aflatoxin B_1, a mycotoxin produced by *Aspergillus flavus* and *Aspergillus parasiticus*, is implicated as a hepatic carcinogen [for reviews, see Garner (1980), Hsieh and Wong (1982), Essigmann et al. (1983), and Busby and Wogan (1984)]. Shimada and Guengerich (1989) reported cytochrome P-450$_{NF}$[1] to be the principal human liver enzyme involved in the bioactivation of aflatoxin B_1; Aoyama et al. (1990) have recently reported that several additional forms of human cytochrome P-450 activate the carcinogen. The probable electrophilic intermediate is aflatoxin B_1 8,9-epoxide, which has been synthesized by oxidation of aflatoxin B_1 with dimethyldioxirane (Baertschi et al., 1988). Alkylation by activated aflatoxin B_1 occurs at guanine N7 to form the cationic DNA adduct 8,9-dihydro-8-(*N*7-guanyl)-9-hydroxyaflatoxin B_1 (Garner et al., 1972; Essigmann et al., 1977; Lin et al., 1977; Croy et al., 1978). The structures of aflatoxin B_1, aflatoxin B_1 8,9-epoxide, and the DNA adduct 8,9-dihydro-8-(*N*7-guanyl)-9-hydroxyaflatoxin B_1 are shown in Figure 1. DNA adduct formation elicits a strong biological response, as measured by *Salmonella typhimurium* reversion (McCann et al., 1975; Wong et al., 1977; Mori et al., 1986; Yourtee et al., 1987) or *umu* gene activation (Oda et al., 1985;

† This research was supported by NIEHS Grants ES03755 and ES00267.

[1] Abbreviations: AFB, aflatoxin B; CD, circular dichroism; DNA, deoxyribonucleic acid; EDTA, ethylenediaminetetraacetic acid; DSS, sodium 4,4-dimethyl-4-silapentanesulfonate; HPLC, high-pressure liquid chromatography; NMR, nuclear magnetic resonance; NOE, nuclear Overhauser enhancement; ppm, parts per million; P-450$_{NF}$, liver microsomal cytochrome P-450 (nifedipine oxidase; Shimada & Guengerich, 1989); TPPI, time-proportional phase increment; UV, ultraviolet; 1D one dimensional; 2D, two dimensional. Unless otherwise noted the oligonucleotides discussed in this paper do not have terminal phosphate groups—we abbreviate the nomenclature for oligonucleotides by leaving out the phosphodiester linkage. A, C, G, and T refer to mononucleotide units, and ^{AFB}G is the aflatoxin B_1 alkylated mononucleotide 8,9-dihydro-8-(*N*7-guanyl)-9-hydroxyaflatoxin B_1. A right superscript refers to numerical position in the oligodeoxynucleotide sequence starting from the 5′-terminus of chain A and proceeding to the 3′-terminus of chain A and then from the 5′-terminus of chain B to the 3′-terminus of chain B. C2, C5, C6, C8, C1′, C2′, C2″, etc., represent specific carbon nuclei. H2, H5, H6, H8, H1′, H2′, H2″, etc., represent the protons attached to these carbons. The modified mononucleotide ^{AFB}G contains two protons labeled H8, located on the guanyl imidazole ring and on the aflatoxin furan ring. They have been designated throughout as either guanine H8 or AFB H8 to avoid confusion.

0006-2960/90/0429-10438$02.50/0

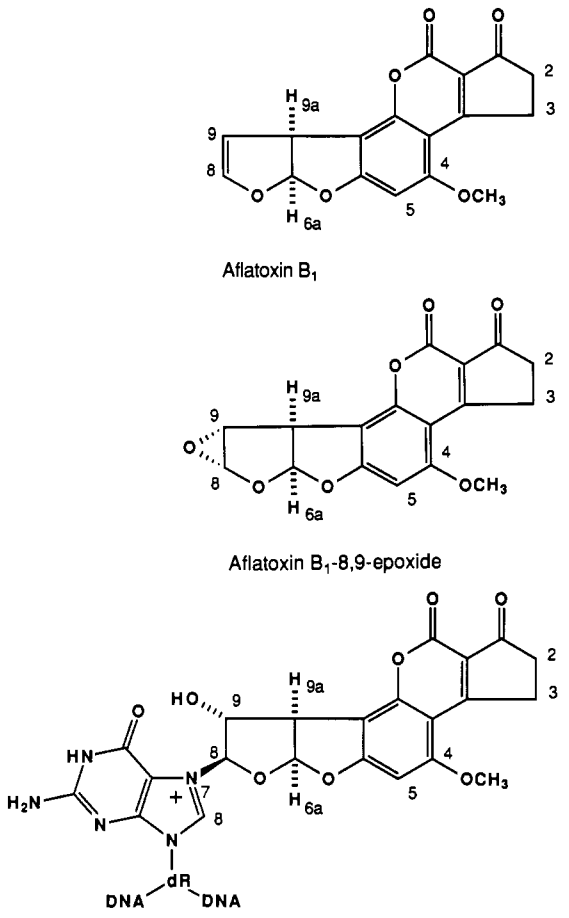

FIGURE 1: Structures of aflatoxin B_1, aflatoxin B_1 8,9-epoxide, and the cationic adduct 8,9-dihydro-8-(*N*7-guanyl)-9-hydroxyaflatoxin B_1 contained within an oligodeoxynucleotide. The aflatoxin protons are numbered to correspond with the NMR data.

Shimada et al., 1987; Baertschi et al., 1989; Shimada & Guengerich, 1989).

Aflatoxin B_1 8,9-epoxide reacts readily with aqueous solutions of deoxyguanosine-containing B-DNA to form 8,9-dihydro-8-(*N*7-guanyl)-9-hydroxyaflatoxin B_1 (Baertschi et al., 1988). Reaction of oligodeoxynucleotides with this epoxide provides a direct method for the preparation of aflatoxin–oligodeoxynucleotide adducts. We previously demonstrated that $d(ATCGAT)_2$ reacts with only 1 equiv of aflatoxin B_1 8,9-epoxide, to form 8,9-dihydro-8-{*N*7-guanyl-[d(ATCGAT)]}-9-hydroxyaflatoxin B_1·d(ATCGAT) (Gopalakrishnan et al., 1989a). We refer to this nonsymmetrical adduct, in which one strand of deoxyguanosine-modified DNA is base-paired to the complementary nonmodified strand, as d(ATC^{AFB}GAT)·d(ATCGAT), where ^{AFB}G designates the modified deoxyguanosine. In the present work, we demonstrate that $d(ATGCAT)_2$, a sequence isomer of $d(ATCGAT)_2$ in which the position of the deoxycytidine and deoxyguanosine have been interchanged, reacts with 2 equiv of aflatoxin B_1 8,9-epoxide. The resulting product is 8,9-dihydro-8-{*N*7-guanyl-[d(ATGCAT)]}-9-hydroxyaflatoxin B_1·8,9-dihydro-8-{*N*7-guanyl-[d(ATGCAT)]}-9-hydroxyaflatoxin B_1, a symmetrical duplex in which two strands of deoxyguanosine-modified DNA are base-paired. We refer to this second adduct as $d(AT^{AFB}GCAT)_2$.

We have utilized ^{1}H NMR spectroscopy to examine the conformation of d(ATC^{AFB}GAT)·d(ATCGAT) and $d(AT^{AFB}GCAT)_2$. Secure spectral assignments for most of the ^{1}H resonances in both adducts have been made. In both cases, specific NOE contacts are observed between the aflatoxin moiety and the oligodeoxynucleotide. These NOEs involve both the major and minor groove of the DNA. Adduct formation results in specific perturbation of internucleotide NOEs which are observed for right-handed oligodeoxynucleotides. Specific changes in chemical shift and spin–lattice relaxation rate are observed for both the aflatoxin and DNA protons. The data reveal that the aflatoxin moiety is intercalated above the 5′-face of the modified guanine in both d(ATC^{AFB}GAT)·d(ATCGAT) and $d(AT^{AFB}GCAT)_2$. The differences in stoichiometry of reaction between aflatoxin B_1 8,9-epoxide and the two oligodeoxynucleotides, and the geometry of the resulting adducts, provide supporting evidence for a reaction mechanism that involves an intercalated transition complex between aflatoxin B_1 8,9-epoxide and B-DNA.

Experimental Procedures

Materials. Aflatoxin B_1 was purchased from Sigma Chemicals, Inc., or Aldrich Chemicals. *Crystalline aflatoxins are extremely hazardous due to their electrostatic nature and should be handled using appropriate containment procedures and respiratory mask to prevent inhalation. Aflatoxins can be destroyed by treatment with commercial NaOCl solutions.* Reagents for oligodeoxynucleotide synthesis were purchased from Pharmacia–PL Biochemicals, Inc. and Fisher Scientific. d(ATCGAT) and d(ATGCAT) were synthesized by using standard solid-phase phosphoramidite chemistry with an automated synthesizer. The amount of single-stranded d(ATCGAT) and d(ATGCAT) was determined by using extinction coefficient of 41 500 M^{-1} cm^{-1} at 260 nm.

Preparation of Aflatoxin B_1 Adducts. Aflatoxin B_1 8,9-epoxide was prepared as described by Baertschi et al. (1988). *It should be assumed that aflatoxin B_1 8,9-epoxide is highly toxic and carcinogenic. Manipulations should be carried out in a well-ventilated hood with suitable containment procedures.* Adducts were prepared by addition of excess aflatoxin B_1 8,9-epoxide in dichloromethane to double-stranded oligodeoxynucleotide at 5 °C. All reactions with aflatoxin B_1 were performed under subdued light to minimize potential formation of aflatoxin B_1 photoproducts or photodecomposition of the resulting carcinogen–DNA adduct (Israel-Kalinsky et al., 1982; Misra et al., 1983; Stark et al., 1990; Shaulsky et al., 1990). A typical reaction and the subsequent purification is described by Gopalakrishnan et al. (1989a). Maintenance of these cationic guanine N7 adducts at <5 °C was essential to minimize depurination at ^{AFB}G. Samples were stored at −20 °C between experiments and were repurified as necessary over the course of the NMR experiments.

Nuclear Magnetic Resonance. ^{1}H NMR frequencies of 300.13, 400.13, and 499.84 MHz were utilized. The oligodeoxynucleotide duplex concentrations ranged from 0.8 to 2.0 mM. Samples were dissolved in 400 μL of NMR buffer consisting of 0.1 M NaCl, 5×10^{-5} M disodium EDTA, and 0.01 M sodium phosphate, pH 7.0. For observation of the exchangeable ^{1}H resonances, buffered samples were dissolved in H_2O containing 10% D_2O. 1D spectra in H_2O were acquired by using the 1331 water suppression pulse sequence (Hore, 1983a,b). A 2D NOESY spectrum in H_2O was acquired by using the 1:1 (jump–return) suppression pulse sequence (Plateu & Gueron, 1982) as developed by Sklenar and Bax (1987) and Sklenar et al. (1987). For observation of the nonexchangeable protons, the buffered samples were lyophilized in triplicate from D_2O, dissolved in 400 μL of 99.96% D_2O, and purged with dry N_2 prior to capping. Nonselective spin–lattice relaxation measurements were performed by using the standard inversion–recovery pulse technique. Phase-sen-

sitive NOESY spectra at 499.84 MHz were recorded at 5 °C using the following parameters: mixing time = 0.100 s, 2K complex data points in t_2, 512 complex data points in t_1, 32 acquisitions per FID, relaxation delay of 3.0 s, sweep width of 5400 Hz in both dimensions, a shifted Gaussian apodization function for t_2, and a shifted sine bell apodization function for the t_1 dimension. The data were zero-filled in t_1 to give 2K × 2K complex data points. The residual solvent resonance was saturated during the relaxation delay. Additional data were collected at 400.13 MHz and 5 °C with various mixing times of 0.100–0.400 s, using the TPPI algorithm (Bodenhausen et al., 1984). Chemical shifts were referenced internally to DSS; sample temperature was controlled within 0.5 °C.

Results

Reaction Stoichiometry. The reaction between aflatoxin B_1 8,9-epoxide and d(ATCGAT)$_2$ is characterized by a limiting stoichiometry of 1:1 aflatoxin B_1:d(ATCGAT)$_2$ to yield the adduct d(ATC^{AFB}GAT)·d(ATCGAT). Formation of this adduct results in a doubling of oligodeoxynucleotide ^{1}H NMR resonances due to loss of strand symmetry (Gopalakrishnan et al., 1989a). The magnitude of the aflatoxin-induced resolution of symmetry-related protons varies, such that for some protons (e.g., the thymine CH_3 protons) loss of symmetry is evidenced only by line broadening. Reaction of the sequence isomer d(ATGCAT)$_2$ with aflatoxin B_1 8,9-epoxide gives a markedly different result: d(ATGCAT)$_2$ reacts with 2 equiv of epoxide to yield the bis adduct d(AT^{AFB}GCAT)$_2$ in which both deoxyguanosines are modified. Formation of d(AT^{AFB}GCAT)$_2$ from d(ATGCAT)$_2$ occurs with retention of pseudodyad symmetry, and no doubling of NMR resonances is observed. The loss of symmetry for d(ATC^{AFB}GAT)·d(ATCGAT) and retention of symmetry for d(AT^{AFB}GCAT)$_2$ are clearly evident in ^{1}H NOESY spectra which are shown in Figure 2. Comparative chromatographic analysis of the respective reaction mixtures is provided in Figure S1 of the supplementary material (see paragraph at the end of this paper regarding supplementary material).

Stability of d(ATC^{AFB}GAT)·d(ATCGAT) and d(AT^{AFB}GCAT)$_2$. Both adducts have increased thermal stability as compared to the parent duplexes. The two unmodified hexamers each exhibit broad melting transitions for which the lower base line is not attained even at 0 °C. In contrast, the appearance of lower base lines is clearly observed for the modified oligodeoxynucleotides. A shift in the midpoint of the melting transition to higher temperature and increased sigmoidal appearance of the plot is observed [for a melting curve of d(ATC^{AFB}GAT)·d(ATCGAT) see Gopalakrishnan et al. (1989a); a melting curve for d(AT^{AFB}GCAT)$_2$ is provided in Figure S2 of the supplementary material]. Sample absorbance at low temperature subsequent to the melting experiment was observed to differ slightly from the value that was recorded prior to heating. HPLC analysis suggested partial depurination occurred during the course of the melting experiment. The mixing of equimolar amounts of d(ATC^{AFB}GAT) and d(ATCGAT) results in spontaneous formation of d(ATC^{AFB}GAT)·d(ATCGAT) (Gopalakrishnan et al., 1989a). The corresponding titration of d(AT^{AFB}GCAT)$_2$ into d(ATGCAT)$_2$ results in the appearance of separate NMR signals arising from equilibrium between (1) the two symmetrical duplexes d(ATGCAT)$_2$ and d(AT^{AFB}GCAT)$_2$ and (2) nonsymmetrical d(AT^{AFB}GCAT)·d(ATGCAT) (shown in Figure S3 of the supplementary material).

^{1}H NMR Spectral Assignments for d(ATC^{AFB}GAT)·d(ATCGAT). (*a*) *Aflatoxin Protons.* The ^{1}H resonances of the aflatoxin moiety fall into three categories: (1) H2α, H2β, H3α, and H3β, located on the cyclopentenone ring,[2] (2) 4-OCH_3 and H5, located on the benzene ring, and (3) H6a, AFB H8, H9, and H9a, located on the fused furofuran ring. These assignments, except for the cyclopentenone ring protons, were reported previously (Gopalakrishnan et al., 1989a). On the cyclopentenone ring, protons H2α and H2β resonate upfield of H3α and H3β. These four signals are identified from inspection of phase-sensitive NOESY spectra (Table I), although they are partially obscured by the deoxyribose H2′ and H2″ resonances which occur in the same general region of the spectrum (Figure 3A). The H2α and H2β resonances are identified by a strong cross-peak (δ 1.50, 1.80 ppm) which is not obscured by the deoxyribose signals. These two signals each exhibit an NOE to resonances at 2.40 and 2.66 ppm, which are identified as H3α and H3β. The absolute assignments (i.e., α vs β) are dependent upon knowledge of the orientation of the aflatoxin moiety in d(ATC^{AFB}GAT)·d(ATCGAT) and d(AT^{AFB}GCAT)$_2$ and are discussed in a subsequent section.

Table I: Chemical Shifts (ppm from DSS) of the Cyclopentenone Ring Protons of Aflatoxin B_1 in d(ATC^{AFB}GAT)·d(ATCGAT) at 5 °C[a]

proton	δ_{free}	δ_{adduct}	$\Delta\delta$
H2α	2.42	1.49	−0.93
H2β	2.42	1.80	−0.62
H3α	3.22	2.41	−0.81
H3β	3.22	2.66	−0.56

[a] Sample concentration was 0.8 mM duplex. Assignments for the remaining aflatoxin protons were reported by Gopalakrishnan et al. (1989a). δ_{free} values are derived from a saturated solution of aflatoxin B_1 in D_2O (Gopalakrishnan et al., 1989b). Negative ppm values of $\Delta\delta$ refer to increased shielding in the adduct as compared to free aflatoxin B_1.

(*b*) *Oligodeoxynucleotide Protons.* Figure 4A shows an expansion of the base-to-H1′ cross-peaks of the phase-sensitive NOESY spectrum obtained at 5 °C for d(ATC^{AFB}GAT)·d(ATCGAT). Inspection of the base-to-H1′ NOE connectivities (Feigon et al., 1983; Hare et al., 1983) shows interruptions only at the central Cp^{AFB}G·CpG sequence. The two 5′-terminal A H8 resonances are located at 8.17 and 8.15 ppm. Each of these protons exhibits only a single NOE to the deoxyribose H1′ region of the spectrum, which corresponds to the intranucleotide NOE to the 5′-terminal A H1′, located at 6.07 and 6.05 ppm. The two 5′-terminal A H1′ resonances exhibit NOEs to the 3′-neighbor T H6 resonances, which are located at 7.41 and 7.45 ppm. The assignment of the 7.41 and 7.45 ppm signals as T H6 resonances is verified by the observation that these signals also exhibit NOEs to T CH_3 protons located at 1.18 ppm. The two T H6 resonances each exhibit intranucleotide NOEs to the T H1′ resonances, located at 5.97 and 5.96 ppm. The two T H1′ resonances exhibit NOEs to their 3′-neighbor C H6 resonances, which are located at 7.76 and 7.64 ppm. The assignments of the C H6 signals are verified by observation of strong cross-peaks between these two signals and the two C H5 signals, located at 5.65 and 5.74 ppm. The two C H1′ resonances are identified from intranucleotide NOEs from the H6 protons and are located at 5.98 and 6.03 ppm.

[2] The definitions of the enantiotopic protons at C2 and C3 are based upon the Cahn, Ingold, and Prelog nomenclature. We defined H2α to be the *pro-R* proton at C2; H2β is defined to be the *pro-S* proton at C2. H3α is defined to be the *pro-S* proton at C3, and H3β is defined to be the *pro-R* proton at C3. H2α and H3α lie on the same face of the cyclopentenone ring as do H6a and H9a; H2β and H3β lie on the other face of the cyclopentenone ring.

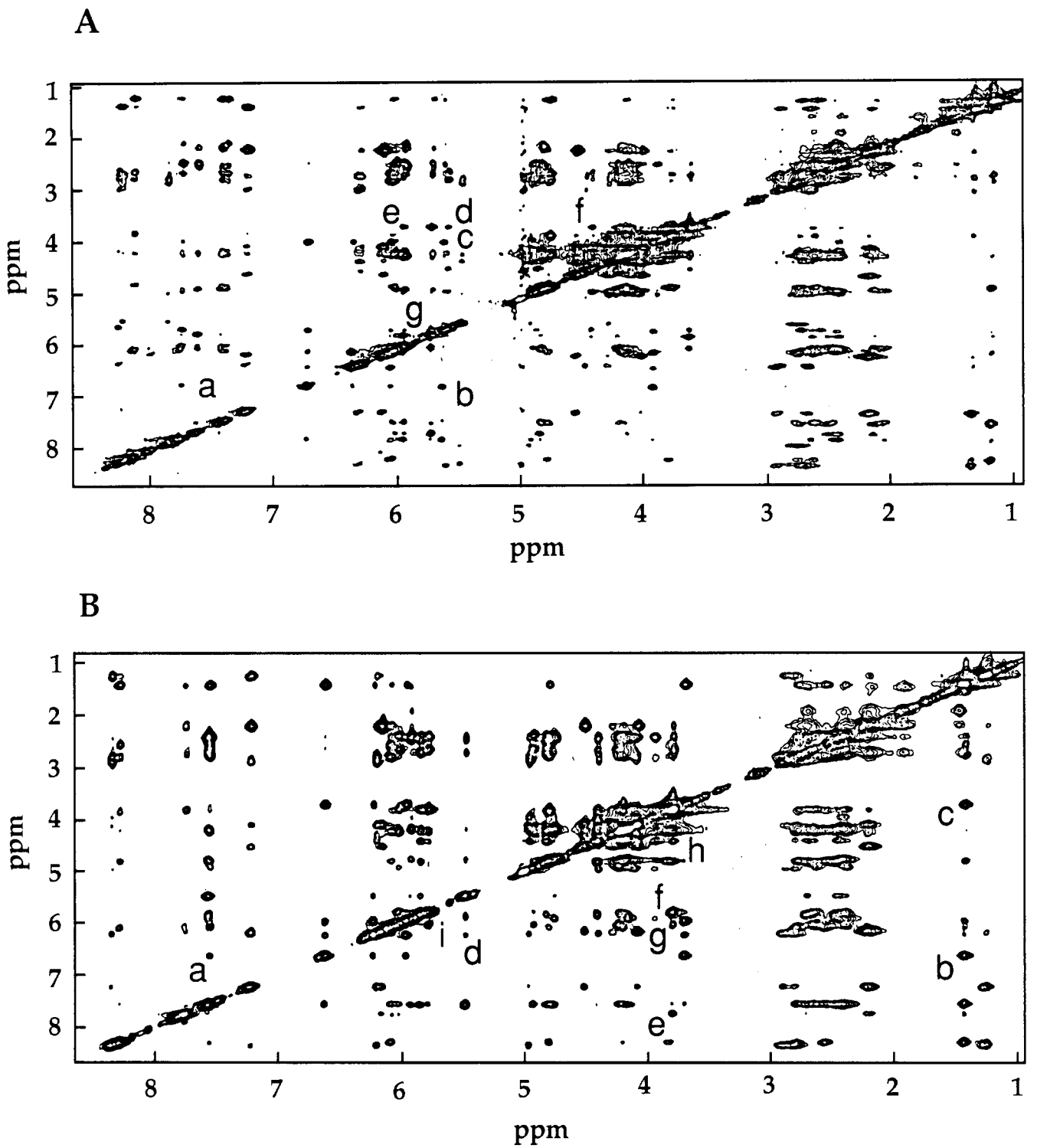

FIGURE 2: NOESY spectra of (A) d(ATC^{AFB}GAT)·d(ATCGAT) and (B) d(AT^{AFB}GCAT)$_2$. A doubling of ^{1}H resonances occurs in d(ATC^{AFB}GAT)·d(ATCGAT). This results from loss of pseudodyad symmetry. These spectra were obtained at 500 MHz in D_2O buffer, 5 °C, with a mixing time of 100 ms. The labeled cross-peaks in the spectra correspond to specific aflatoxin B_1–DNA NOEs and are cross-referenced in Tables III and IV. Key to cross-peaks for d(ATC^{AFB}GAT)·d(ATCGAT) (A): a, ^{AFB}G^4 H6a–C^3 H6; b, ^{AFB}G^4 H6a–C^3 H5; c, ^{AFB}G^4 H9a–C^3 H5; d, e, f, ^{AFB}G^4 4-OCH$_3$–^{AFB}G^4 H1′, C^3 H1′, ^{AFB}G^4 H4′; g, AFB H5–C^3 H1′. Key to cross-peaks for d(AT^{AFB}GCAT)$_2$ (B): a, ^{AFB}G^3 H6a–T^2 H6; b, ^{AFB}G^3 H6a–T^2 CH$_3$; c, ^{AFB}G^3 H9a–T^2 CH$_3$; d, AFB H8–C^4 H5; e, f, g, h, ^{AFB}G^3 4-OCH$_3$–A^5 H2, ^{AFB}G^3 H1′, T^2 H1′, ^{AFB}G^3 H4′; i, AFB H5–T^2 H1′. For AFB numbering scheme, see Figure 1.

At this point, the pattern of sequential connectivities is lost. ^{AFB}G^4 guanine H8 is not observed in D_2O buffer because formation of the cationic adduct at ^{AFB}G^4 N7 results in exchange of this proton with solvent. No conclusion regarding the sequential connectivity between C^{3}H1′ and ^{AFB}G^4 guanine H8 can be made from Figure 4A. There is also no connectivity observed between C^9 H1′ and G^{10} H8. Adduct formation has perturbed this sequential connectivity in the complementary strand of d(ATC^{AFB}GAT)·d(ATCGAT). Thus, partial sequential connectivities proceeding from the 5′-terminus of each strand have been identified. The assignments for one strand are arranged AH8 (8.17 ppm)–AH1′ (6.07 ppm)–TH6 (7.41 ppm)–TH1′ (5.97 ppm)–CH6 (7.76 ppm)–CH1′ (5.98 ppm) and, for the other strand, are arranged AH8 (8.15 ppm)–AH1′ (6.05 ppm)–TH6 (7.45 ppm)–TH1′ (5.96 ppm)–CH6 (7.64 ppm)–CH1′ (6.03 ppm).

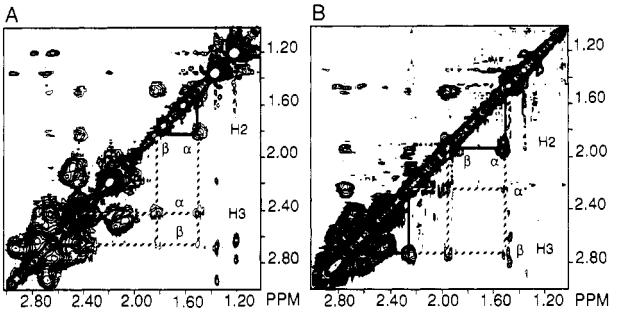

FIGURE 3: Identification of the cyclopentenone ring resonances of aflatoxin B_1 in (A) d(ATC^{AFB}GAT)·d(ATCGAT) and (B) d(AT^{AFB}GCAT)$_2$. Strong cross-peaks arising from cross-relaxation between the geminal H2 α,β and H3 α,β are observed; the H2 signals are upfield of the H3 signals. Weaker NOEs are observed between the vicinal protons, as indicated by the dotted lines. The H3 α and β resonances are obscured by the deoxyribose H2′ and H2″ resonances. In the upper right corner are the thymine CH_3 signals. The assignment of the H3 signals is based upon observation of an NOE between aflatoxin H3α and A^5 H2 in d(AT^{AFB}GCAT)$_2$; the assignment of the H2 signals is based upon observation of an NOE between H2β and C H1′ of the modified base pair C·^{AFB}G, as described in the text. Note the increased shielding for aflatoxin H3α in d(AT^{AFB}GCAT)$_2$ as compared to d(ATC^{AFB}GAT)·d(ATCGAT). For AFB numbering scheme, see Figure 1. The phase-sensitive NOESY spectra were recorded at 400 MHz, 5 °C, with a mixing time of 100 ms.

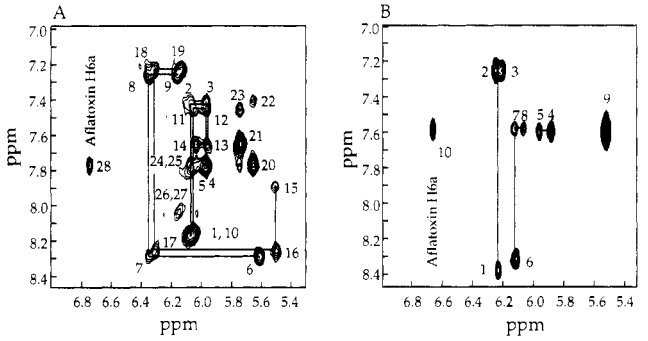

FIGURE 4: Sequential base–H1′ NOE connectivities for (A) d(ATC^{AFB}GAT)·d(ATCGAT) and (B) d(AT^{AFB}GCAT)$_2$. The solid lines in each NOESY panel represent intrastrand sequential connectivities between base protons and deoxyribose H1′ protons. No cross-peaks are observed from ^{AFB}G guanine H8 due to exchange with deuteriated buffer. The sequential intrastrand NOEs are perturbed in the complementary strand due to the presence of ^{AFB}G. Thus for d(ATC^{AFB}GAT)·d(ATCGAT) there is no connectivity between G^{10} H8 and C^9 H1′ (panel A), and for d(AT^{AFB}GCAT)$_2$ there is no connectivity between A^5 H8 and C^4 H1′ (panel B). Cross-peaks 24–27 in (A) are suggestive of terminal base pair fraying in d(ATC^{AFB}GAT)·d(ATCGAT). The phase-sensitive NOESY spectra were recorded at 500 MHz, 5 °C, with a mixing time of 100 ms. Key to cross-peaks in Figure 4A: 1, A^1 H8–A^1 H1′; 2, A^1 H1′–T^2 H6; 3, T2 H6–T^2 H1′; 4, T^2 H1′–C^3 H6; 5, C^3 H6–C^3 H1′; 6, ^{AFB}G^4 H1′–A^5 H8; 7, A^5 H8–A^5 H1′; 8, A^5 H1′–T^6 H6; 9, T^6 H6–T^6 H1′; 10, A^7 H8–A^7 H1′; 11, A^7 H1′–T^8 H6; 12, T^8 H6–T^8 H1′; 13, T^8 H1′–C^9 H6; 14, C^9 H6–C^9 H1′; 15, G^{10} H8–G^{10} H1′; 16, G^{10} H1′–A^{11} H8; 17, A^{11} H8–A^{11} H1′; 18, A^{11} H1′–T^{12} H6; 19, T^{12} H6–T^{12} H1′; 20, C^3 H5–C^3 H6; 21, C^9 H5–C^9 H6; 22, C^3 H5–T^2 H6; 23, C^9 H5–T^8 H6; 24, A^1 H2–A^1 H1′; 25, A^7 H2–A^7 H1′; 26, A^5 H2–T^{6}H1′; 27, A^{11} H2–T^{12}H1′; 28, ^{AFB}G^4 H6a–C^3 H6. Key to cross-peaks in Figure 4B: 1, A^1 H8–A^1 H1′; 2, A^1 H1′–T^2 H6; 3, T^2 H6–T^2 H1′; 4, ^{AFB}G^3 H1′–C^4 H6; 5, C^4 H6–C^4 H1′; 6, A^5 H8–A^5 H1′; 7, A^5 H1′–T^6 H6; 8, T^6 H6–T^6 H1′; 9, C^4 H5–C^{4}H6; 10, ^{AFB}G^3 H6a–T^{2}H6. For AFB numbering scheme, see Figure 1.

These NOE connectivities cannot differentiate between the two strands of the modified duplex, since each strand has the same sequence (Krugh et al., 1989). Strand assignment is based upon identification of spectroscopic markers (e.g., ligand–DNA NOEs) which are unique to either the modified or unmodified strand.[3] Observation of an NOE between H6a of aflatoxin and one C H6, located at 7.76 ppm (Figure 2A, cross-peak a; Figure 4A, cross-peak 28), provides a basis for the strand assignments of the modified duplex beginning at the two 5′-A termini, and proceding to C^3 and C^9, respectively. This NOE could only be observed between aflatoxin H6a and C^3 H6.

The two 3′-terminal T H1′ signals are observed at 6.13 and 6.15 ppm. Each of these protons exhibits an intranucleotide NOE to the 3′-terminal T H6 resonances, located at 7.24 and 7.22 ppm. Assignment of the latter two signals as arising from T H6 is verified by observation of NOEs between these two protons and T CH_3 protons, located at 1.33 ppm. The two T H6 exhibit connectivity to their respective 5′-neighbor A H1′ resonances, which are observed at 6.31 and 6.34 ppm. Intranucleotide NOEs are observed between the two A H1′ protons and the two A H8 protons, located at 8.29 and 8.25 ppm. The two A H8 resonances exhibit connectivity to the 5′-neighbor G H1′ resonances, located at 5.61 and 5.50 ppm. The sequential connectivities for the two strands of d(ATC^{AFB}GAT)·d(ATCGAT) beginning from the 3′-termini are TH1′ (6.13 ppm)–TH6 (7.24 ppm)–AH1′ (6.31 ppm)–AH8 (8.29 ppm)–GH1′ (5.61 ppm) and TH1′ (6.15 ppm)–TH6 (7.22 ppm)–AH1′ (6.34 ppm)–AH8 (8.25 ppm)–GH1′ (5.50 ppm).

The observation that ^{AFB}G^4 guanine H8 exchanges with solvent due to increased acidity upon formation of the cationic N7 adduct provides the basis for determination of strand identity. In deuteriated buffer, an intranucleotide NOE between G H8 and G H1′ can only be observed for the unmodified strand. Inspection of Figure 4A demonstrates that one strand exhibits this NOE between G^{10} H8 and G^{10} H1′ (cross-peak 15), which assigns G^{10} H8 at 7.89 ppm and securely establishes the assignment of the modified and unmodified strands. Identification of the 12 deoxyribose spin systems to yield assignments for the remaining deoxyribose protons proceeded from phase-sensitive NOESY data.

The spectral assignments for the d(ATC^{AFB}GAT)·d(ATCGAT) oligodeoxynucleotide protons are summarized in Table T1 of the supplementary material. Figure S5, panel A (in the supplementary material), details the NOE cross-peaks observed between deoxyribose H2′, H2″, deoxyribose H1′, and purine H8/pyrimidine H6 and reveals a pattern of missing cross-peaks which correspond to the missing cross-peaks of Figure 4A.

Resonances arising from six hydrogen-bonded imino protons are observed in four peaks located between 12 and 14.2 ppm. Two peaks of area two protons each are observed at 14 and 13.4 ppm. Of these two peaks, the 13.4 ppm signal is broadened as compared to the 14 ppm signal. Two additional signals, each corresponding to one proton, are observed at 12 and 13.2 ppm. Figure 5 shows the results of a series of NOE difference experiments from which the imino signals of d(ATC^{AFB}GAT)·d(ATCGAT) were assigned. Irradiation of the broad resonance located at 13.4 ppm assigned as the

[3] It is assumed that adduct formation does not severely perturb the right-handed conformation of the oligodeoxynucleotide. Stoichiometric considerations demonstrate that the adduct consists of one strand of unmodified d(ATCGAT) and one strand of the modified oligodeoxynucleotide d(ATC^{AFB}GAT). The CD spectrum of d(ATC^{AFB}GAT)·d(ATCGAT) is consistent with a right-handed helix. Formation of this adduct is accompanied by net thermodynamic stabilization and retention of six NH–N hydrogen bonds between base pairs (Gopalakrishnan et al., 1989a). NOE contacts are observed between the thymine CH_3 protons and adenine H8 protons of the terminal and penultimate A·T base pairs. These NOEs suggest normal stacking interactions between the terminal base pairs.

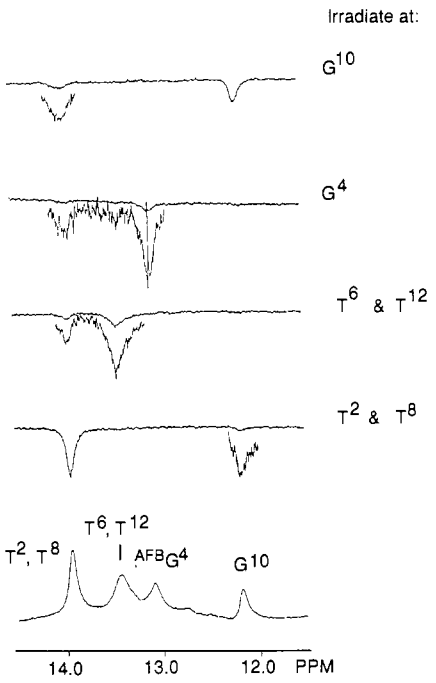

FIGURE 5: Assignment of the imino protons of d(ATC^{AFB}GAT)·d(ATCGAT) by NOE difference spectroscopy. Note that irradiation of either $^{AFB}G^4$ H1 or G^{10} H1 results in observation of an NOE to the internal A·T imino protons T^2 H3 and T^8 H3 but not to the neighbor G·C imino proton, $^{AFB}G^4$ H1 or G^{10} H1. Aflatoxin modification eliminates the NOE between the imino proton of the modified base pair and the imino proton of the 5′-neighbor base pair. The NOE difference spectra of d(ATC^{AFB}GAT)·d(ATCGAT) were acquired at −5 °C where $^{AFB}G^4$ H1 is clearly resolved.

terminal thymine H3 protons shows an NOE only to the set of imino protons located at 14 ppm, which are assigned as the internal thymine H3 protons. Irradiation of the 14.0 ppm signal fails to give the reciprocal NOE to the broad peak at 13.4 ppm, presumably because of increased exchange of the terminal thymine H3 protons with solvent. However, irradiation at 14 ppm does reveal NOEs to two signals located at 8.02 and 8.04 ppm, which are assigned as A^5 H2 and A^{11} H2. Irradiation at 14 ppm also gives an NOE to the signal located at 12 ppm, assigned as a guanine H1. The reverse experiment, in which the 12 ppm signal is irradiated, gives an NOE to the signal at 14 ppm. Irradiation of the remaining signal at 13.2 ppm, which is assigned as the other guanine H1, also shows an NOE to the 14 ppm signal. Of the two guanine H1 signals, the 13.2 ppm signal is assigned as $^{AFB}G^4$ H1. This assignment is based upon the rationale that adduct formation at guanine N7 should result in increased acidity for $^{AFB}G^4$ H1. This signal is shifted downfield and has increased line width as compared to G^{10} H1 observed at 12 ppm and G H1 of unmodified $d(ATCGAT)_2$. No NOE is observed between $^{AFB}G^4$ H1 and G^{10} H1; each shows connectivity only to an internal T H3. A sharp signal is observed at 9.75 ppm, which integrates as one proton, and is assigned as $^{AFB}G^4$ guanine H8 from NOESY data in H_2O obtained for $d(AT^{AFB}GCAT)_2$. No NOE connectivity is observed between the 9.75 ppm signal and the hydrogen-bonded imino signals observed between 12 and 14.2 ppm.

^1H NMR Spectral Assignments for $d(AT^{AFB}GCAT)_2$. (*a*) *Aflatoxin Protons.* The assignment of the aflatoxin protons in $d(AT^{AFB}GCAT)_2$ follows along similar lines to the above discussion. Figures 4B and S4, panel B (supplementary material), detail these assignments. The chemical shifts of the aflatoxin B_1 resonances summarized in Table II are similar, but not equivalent, to those observed in d(ATC^{AFB}GAT)·d(ATCGAT) (Gopalakrishnan et al., 1989a). These differences presumably result from changes in the microenvironment of the aflatoxin moiety in the two adducts.

Table II: Chemical Shifts (ppm from DSS) of Aflatoxin B_1 Protons in $d(AT^{AFB}GCAT)_2$ at 5 °C[a]

proton	δ_{free}	δ_{adduct}	$\Delta\delta$
H2α	2.42	1.51	−0.91
H2β	2.42	1.94	−0.48
H3α	3.22	2.22	−1.00
H3β	3.22	2.73	−0.59
4-OCH_3	3.98	3.81	−0.17
H5	6.69	5.80	−0.89
H6a	6.93	6.65	−0.28
H8	6.59	6.26	−0.33[b]
H9	5.57	5.98	+0.41[b]
H9a	4.80[c]	3.71	−1.09[c]

[a] Sample concentration was 1.2 mM duplex. δ_{free} values are derived from a saturated solution of aflatoxin B_1 in D_2O (Gopalakrishnan et al., 1989b). Negative ppm values of $\Delta\delta$ refer to increased shielding in the adduct as compared to free aflatoxin B_1. [b] Change in hybridization at carbons C8 and C9 upon epoxidation and formation of adduct to guanine N7. [c] In sample of free aflatoxin B_1, this proton resonance is obscured by residual HDO in the sample.

(*b*) *Oligodeoxynucleotide Protons.* Figure 4B shows the base-to-H1′ region of the phase-sensitive NOESY spectrum for $d(AT^{AFB}GCAT)_2$. Each NOE cross-peak represents two protons which are magnetically equivalent due to the presence of the pseudodyad symmetry axis for this adduct. Two T H6 resonances are identified at 7.57 and $d(AT^{AFB}GCAT)_2$ ppm, on the basis of NOEs observed between T H6 and the corresponding T CH_3 signals, located at 1.45 and 1.26 ppm. Each T H6 resonance exhibits an intranucleotide NOE to a T H1′ resonance, which are identified at 6.05 and 6.18 ppm. Each T H6 resonance also shows connectivity to a 5′-neighbor A H1′ resonance. The two A H8 resonances are identified from A H1′–A H8 cross-peaks, located at 8.32 and 8.38 ppm. $^{AFB}G^3$ guanine H8 is not observed in the spectrum due to exchange with D_2O. The two sets of ApT connectivities (i.e., A^1pT^2 and A^5pT^6) are identified on the basis of observation of an NOE cross-peak between aflatoxin H6a and one thymine H6 (Figure 2B, cross-peak a; Figure 4B, cross-peak 10). Since the adduct is at $^{AFB}G^3$ N7, this NOE could only occur between aflatoxin H6a and T^2 H6. C^4 H6 is identified at 7.59 ppm on the basis of the large cross-relaxation signal observed to C^4 H5 at 5.50 ppm. C^4 H6 exhibits an NOE to C^4 H1′ and also to $^{AFB}G^3$ H1′. In the B conformation, the C^4 base protons H5 and H6 are each predicted to be closer to $^{AFB}G^3$ H1′ than to C^4 H1′. A stronger NOE is observed between both C^4 H5 and C^4 H6, and the H1′ proton located at 5.86 ppm, which is accordingly assigned to $^{AFB}G^3$ H1′, while the resonance at 5.94 ppm is assigned as C^4 H1′. This assignment is confirmed by observation of an NOE between both C^4 H5 and C^4 H6, and C^4 H3′. In agreement with this assignment, a NOESY experiment in H_2O buffer (not shown) revealed the presence of a cross-peak between $^{AFB}G^3$ guanine H8 at 9.75 ppm and $^{AFB}G^3$ H2′,H2″, located at 2.49 and 2.73 ppm, respectively. No NOE connectivity is observed between C^4 and A^5. Three discrete sets of sequential connectivity for $d(AT^{AFB}GCAT)_2$ are observed: A^1 H8 (8.32 ppm)–A^1 H1′ (6.05 ppm)–T^2 H6 (7.57 ppm), A^5 H8 (8.38 ppm)–A^5 H1′ (6.18 ppm)–T^6 H6 (7.24 ppm), and $^{AFB}G^3$H1′ (5.86 ppm)–C^4 H6 (7.59 ppm)–C^4 H1′ (5.94 ppm). Formation of $d(AT^{AFB}GCAT)_2$ causes the pattern of sequential NOESY connectivities to appear as if three dinucleotide units are present: ApT, ^{AFB}GpC, and ApT. These assignments for the oligodeoxynucleotide protons of $d(AT^{AFB}GCAT)_2$ are collected in Table T2 of the supplementary material.

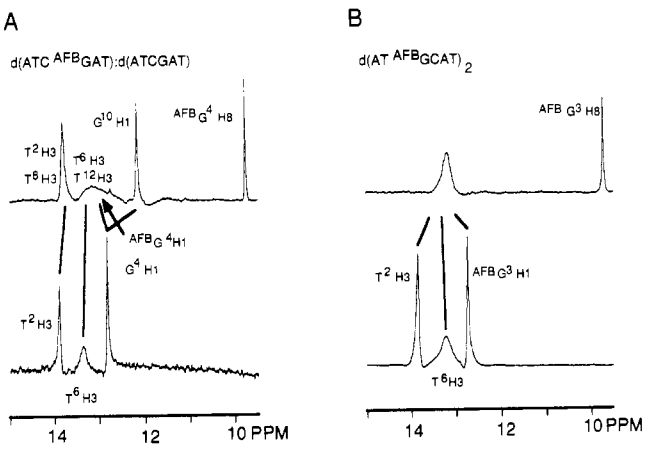

FIGURE 6: For both (A) d(ATC^{AFB}GAT)·d(ATCGAT) and (B) d(AT^{AFB}GCAT)$_2$, similar chemical shift changes of the imino protons are observed. Modification results in a downfield shift and broadening of ^{AFB}G H1 and an upfield shift of the 5′-neighbor base pair imino proton, which is G^{10} H1 in the case of d(ATC^{AFB}GAT)·d(ATCGAT) and T^2 H3 in the case of d(AT^{AFB}GCAT)$_2$. In panels A and B note the presence of a sharp signal at ~9.75 ppm, which is assigned as the guanine H8 proton of ^{AFB}G.

The base-paired imino protons of d(ATGCAT)$_2$ are observed as three resonances (Patel, 1974; Hilbers & Patel, 1975), each of which corresponds to two protons. Upon formation of d(AT^{AFB}GCAT)$_2$, a single broadened resonance corresponding to 6 imino protons is observed at 13.2 ppm (Figure 6B). Irradiation of the 13.2 ppm signal reveals an NOE to the two sets of adenine H2 protons, located at 7.77 and 7.75 ppm. No NOE is observed between the imino protons of d(AT^{AFB}GCAT)$_2$ and the ^{AFB}G^3 guanine H8 resonance of area two protons observed at 9.75 ppm. Comparison of panels A and B in Figure 6 shows that similar changes occur for corresponding imino protons of d(ATCGAT)$_2$ and d(ATGCAT)$_2$ upon formation of d(ATC^{AFB}GAT)·d(ATCGAT) and d(AT^{AFB}GCAT)$_2$, respectively. In both cases, the imino proton of ^{AFB}G shifts downfield and broadens, while the imino proton of the 5′-neighbor base pair shifts upfield. For d(AT^{AFB}GCAT)$_2$, these changes result in a single broadened signal observed at 13.2 ppm, the result of a downfield shift and broadening of the ^{AFB}G^3 H1 resonance, an upfield shift of the T^2 H3 resonance, and little or no perturbation of the T^6 H3 resonance.

Aflatoxin-to-DNA NOEs. For ^{AFB}G^4 of d(ATC^{AFB}GAT)·d(ATCGAT), intranucleotide NOEs are observed between the 4-OCH$_3$ and H5 protons of the aflatoxin moiety, and the deoxyribose. Internucleotide NOEs are observed between 4-OCH$_3$, H5, H6a, and H9a of the aflatoxin moiety in ^{AFB}G^4 and the 5′-neighbor base pair, C^3·G^{10}. The 4-OCH$_3$ and H5 protons of ^{AFB}G^4 exhibit NOEs to C^3 H1′ and ^{AFB}G^4 H1′; 4-OCH$_3$ also shows an intranucleotide NOE to ^{AFB}G^4 H4′. Aflatoxin H6a and H9a exhibit internucleotide NOEs to C^3 H5, and H6a also shows an NOE to C^3 H6. A weak NOE is observed between a cyclopentenone ring proton at C2 of aflatoxin and C^9 H1′. These NOEs are summarized in Table III.

For ^{AFB}G^3 of d(AT^{AFB}GCAT)$_2$, intranucleotide NOEs are observed between the 4-OCH$_3$ and H5 protons of the aflatoxin moiety and deoxyribose, and (in H$_2$O buffer) between AFB H8 and ^{AFB}G^3 guanine H8. Internucleotide NOEs are observed between 4-OCH$_3$, H5, H6a, and H9a of the aflatoxin moiety in ^{AFB}G^3 and the 5′-neighbor base pair, T^2·A^5. The 4-OCH$_3$ protons exhibit NOEs to T^2 H1′, ^{AFB}G^3 H1′, and ^{AFB}G^3 H4′; 4-OCH$_3$ also shows an internucleotide NOE to A^5 H2. NOEs are also observed between aflatoxin H5 and T^2 H1′, T^2 H2″, and T^2 H2′. The last cross-peak is likely a second-order NOE resulting from spin diffusion in the 100-ms data.[4] Additional interactions are observed between an aflatoxin cyclopentenone ring proton at C3 and A^5 H2, and between an aflatoxin cyclopentenone ring proton at C2 and C^4 H1′. Aflatoxin H6a and H9a exhibit internucleotide NOEs to T^2 CH$_3$, and H6a also shows an NOE to T^2 H6. Aflatoxin H8 shows an NOE in the 3′-direction to C^4 H5. These NOEs are summarized in Table IV.

Table III: Summary of NOEs Observed between the Aflatoxin Moiety and the Oligodeoxynucleotide in d(ATC^{AFB}GAT)·d(ATCGAT)

aflatoxin proton of ^{AFB}G^4	alfatoxin–DNA NOEs	figure reference
H2α		
H2β	C^9 H1′	weak NOE obsd at 500 MHz
H3α		
H3β		
4-OCH$_3$	C^3 H1′	Figure 2A, cross-peak e
		Figure S4, panel A, cross-peak a
	^{AFB}G^4 H1′	Figure 2A, cross-peak d
		Figure S4, panel A, cross-peak b
	^{AFB}G^4 H4′	Figure 2A, cross-peak f
		Figure S4, panel A, cross-peak c
H5	C^3 H1′	Figure 2A, cross-peak g
		Figure S4, panel A, cross-peak d
	C^3 H2″	Figure S5, panel A, cross-peak 67
H6a	C^3 H6	Figure 2A, cross-peak a
		Figure 4A, cross-peak 28
	C^3 H5	Figure 2A, cross-peak b
H8		
H9		
H9a	C^3 H5	Figure 2A, cross-peak c
		Figure S4, panel A, cross-peak e

Table IV: Summary of NOEs Observed between the Aflatoxin Moiety and the Oligodeoxynucleotide in d(AT^{AFB}GCAT)$_2$

aflatoxin proton of ^{AFB}G^3	aflatoxin–DNA NOEs	figure reference
H2α		
H2β	C^4 H1′	Figure S5, panel B, cross-peak 35
H3α	A^5 H2	Figure S5, panel B, cross-peak 17
H3β		
4-OCH$_3$	A^5 H2	Figure 2B, cross-peak e
	^{AFB}G^3 H1′	Figure 2B, cross-peak f
	^{AFB}G^3 H4′	Figure 2B, cross-peak h
	T^2 H1′	Figure 2B, cross-peak g
		Figure S4, panel B, cross-peak a
H5	T^{2}H1′	Figure 2B, cross-peak i
		Figure S4, panel B, cross-peak b
	T^{2}H2′	Figure S5, panel B, cross-peak 33 could be spin diffusion
	T^2 H2″	Figure S5, panel B, cross-peak 34
H6a	T^2 H6	Figure 2B, cross-peak a
		Figure 4B, cross-peak 10
	T^2 CH$_3$	Figure 2B, cross-peak b
H8	C^4 H5	Figure 2B, cross-peak d
	^{AFB}G^3 guanine H8	obsd in H$_2$O solution only
H9		
H9a	T^2 CH$_3$	Figure 2B, cross-peak c

Nonselective Spin–Lattice Relaxation. Measurements of nonselective T_1 relaxation for d(ATC^{AFB}GAT)·d(ATCGAT) and d(AT^{AFB}GCAT)$_2$ are collected in Tables T3 and T4 (supplementary material). Figure 7 shows T_1 data for d(ATC^{AFB}GAT)·d(ATCGAT) and d(AT^{AFB}GCAT)$_2$ at a τ value which is close to the T_1 null point for most of the oli-

[4] Spin diffusion contributes to the intensities of the NOE cross-peaks observed at 0.1-s mixing time. The presence of spin diffusion affects quantitative measurement of NOEs but is not expected to alter the overall pattern of NOEs which we observe.

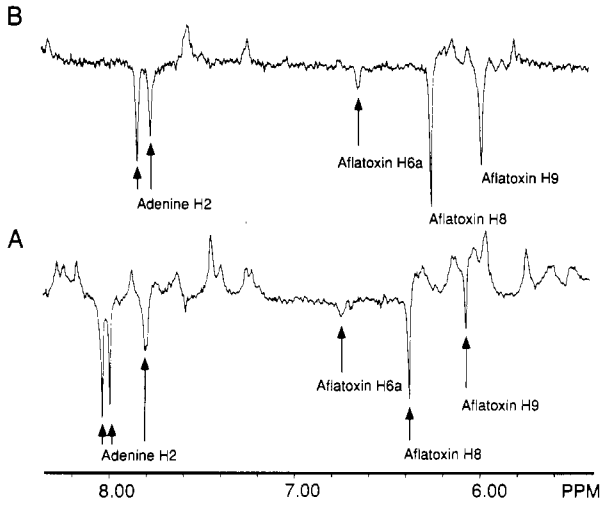

FIGURE 7: Nonselective spin–lattice relaxation data for (A) d(AT-C^{AFB}GAT)·d(ATCGAT) and (B) d($AT^{AFB}GCAT)_2$. The spectra were obtained at 400 MHz, 5 °C, and represent τ values at which most of the oligodeoxynucleotide protons are close to the null point. The slowly relaxing adenine H2 protons are located in the minor groove of the modified oligodeoxynucleotide, whereas aflatoxin protons H8 and H9 face into the major groove of the modified oligodeoxynucleotide. Aflatoxin H6a also faces into the major groove and exhibits a slightly slower T_1 relaxation rate. The spin–lattice relaxation rate of adenine H2 protons in the modified oligodeoxynucleotides is increased but remains slower than for the other oligodeoxynucleotide protons (see Tables T3 and T4, supplementary material).

godeoxynucleotide protons. The inverted signals represent those protons that undergo spin–lattice relaxation more slowly. In addition to the adenine H2 protons, aflatoxin H8 and H9 also show slow spin–lattice relaxation in both oligodeoxynucleotide adducts. Aflatoxin H6a also appears as an inverted signal at this τ value. Adduct formation results in increased relaxation rate for the adenine H2 protons as compared to the unmodified duplexes (Table T3 and T4 in the supplementary material). The greatest alteration of T_1 relaxation is observed for A^5 H2 of d($AT^{AFB}GCAT)_2$.

Chemical Shift Changes upon Adduct Formation. With the exception of aflatoxin H9, formation of either d(AT-C^{AFB}GAT)·d(ATCGAT) or d($AT^{AFB}GCAT)_2$ results in increased shielding for aflatoxin protons as compared to free aflatoxin B_1 [Gopalakrishnan et al. (1989a); Tables I and II]. Adduct formation results in substantial upfield chemical shift changes for aflatoxin H2α,β, H3α,β, 4-OCH_3, H5, H6a, and H9a, the largest shifts of approximately 1.0 ppm being observed for aflatoxin H2α, H3α, H5, and H9a. Chemical shift perturbations of the DNA protons upon adduct formation are limited to the modified C·^{AFB}G base pair and its 5′-neighbor base pair and are summarized in Tables T5 and T6 (supplementary material). The imino proton of the 5′-neighbor base pair shifts upfield upon adduct formation. In contrast, downfield shifts are observed for C^3 H6 and C^9 H6 in d(AT-C^{AFB}GAT)·d(ATCGAT), and T^2 H6 and C^4 H6 in d($AT^{AFB}GCAT)_2$. Increased shielding is observed for the terminal adenine H2 protons in both modified oligodeoxynucleotides. That chemical shift changes arising from aflatoxin adduct formation are localized to the immediate vicinity of the modified base pair provides support for the notion that adduct formation occurs without long-range alteration of B-DNA.

Discussion

The preparation of d($ATC^{AFB}GAT$)·d(ATCGAT) and d($AT^{AFB}GCAT)_2$ provides a striking example of the ability of DNA sequence to mediate aflatoxin B_1 adduct formation at deoxyguanosine N7. Whereas only one molecule of aflatoxin B_1 8,9-epoxide will react with d(ATCGAT)$_2$, two molecules of aflatoxin B_1 8,9-epoxide will react with d-(ATGCAT)$_2$. ^{1}H NMR demonstrates that d(AT-C^{AFB}GAT)·d(ATCGAT) does not undergo disproportionation to d(ATCGAT)$_2$ and d($ATC^{AFB}GAT$) (Gopalakrishnan et al., 1989a) and that d($AT^{AFB}GCAT)_2$ forms a stable duplex.

Intercalation of the Aflatoxin B_1 Moiety. Analysis of the NMR data leads to the conclusion that the aflatoxin B_1 moiety is intercalated above the 5′-face of guanine in ^{AFB}G for both d($ATC^{AFB}GAT$)·d(ATCGAT) and d($AT^{AFB}GCAT)_2$. In this orientation, the overall conformation of the DNA remains right-handed, and the principal alteration of the B-DNA structure occurs adjacent to the binding site at guanine N7 of ^{AFB}G. The aflatoxin methoxy and cyclopentenone ring protons face into the minor groove of the DNA, whereas the furofuran ring protons face into the major groove of the DNA. Evidence in support of this conclusion accrues from inspection of (1) DNA–DNA NOE connectivities, (2) aflatoxin B_1–DNA NOE connectivities, (3) spin–lattice relaxation measurements, and (4) chemical shift perturbations of aflatoxin B_1 protons.

(1) The presence of ^{AFB}G in either d($ATC^{AFB}GAT$)·d(ATCGAT) or d($AT^{AFB}GCAT)_2$ results in specific disturbances of the intrastrand base-to-deoxyribose NOE connectivities characteristic of B-DNA (Feigon et al., 1983; Hare et al., 1983). Perturbation of these connectivities occurs on the 5′-side of ^{AFB}G and affects both the modified strand and the complementary strand. For d($AT^{AFB}GCAT)_2$, an NOE is observed between $^{AFB}G^3$ guanine H8 at 9.75 ppm and $^{AFB}G^3$ H2′,H2″, but no NOE is observed to T^2 deoxyribose protons.[5] The effect on the complementary strand is evident in Figures 4 (base–H1′ connectivities) and S5 (base–H2′,H2″ connectivities; supplementary material). In d($ATC^{AFB}GAT$)·d(ATCGAT) no NOE is observed between G^{10} H8 and C^9 deoxyribose, as evidenced by an interruption between cross-peaks 14 and 15 in Figure 4A (and between cross-peaks 28 and 29, panel A, Figure S5). Likewise, in d($AT^{AFB}GCAT)_2$, no NOE is observed between A^5 H8 and C^4 deoxyribose (see Figure 4B where there is an interruption between cross-peaks 5 and 6, and cross-peaks 10 and 11, panel B, Figure S5). These observations demonstrate that ^{AFB}G perturbs both strands of the modified oligodeoxynucleotide and suggest that the aflatoxin moiety lies on the 5′-face of the modified base pair. The NOE between the imino proton of ^{AFB}G and the imino proton of its 5′-neighbor is also missing, as is demonstrated in Figure 5. Irradiation of either $^{AFB}G^4$ H1 or G^{10} H1 in d($ATC^{AFB}GAT$)·d(ATCGAT) results in observation of an NOE to the imino proton of the 3′-neighbor A·T base pair (at T^2 H3 or T^8 H3) but not to the imino proton of the 5′-neighboring G·C base pair. The lack of an NOE between G^{10} H1 and $^{AFB}G^4$ H1 supports the notion that the aflatoxin moiety lies on the 5′-face of the modified base pair.[6]

(2) Aflatoxin B_1–DNA NOE connectivities are localized to the 5′-neighbor base pair relative to ^{AFB}G and involve both

[5] This NOESY experiment was performed in 90% H_2O buffer to enable observation of $^{AFB}G^3$ guanine H8 which exchanges with solvent. The expected NOE between $^{AFB}G^3$ guanine H8 and $^{AFB}G^3$ H1′ was not observed in this experiment, possibly due to its close proximity to the excitation null centered at the large water signal. The corresponding NOESY experiment in 90% H_2O was not performed on d(AT-C^{AFB}GAT)·d(ATCGAT).

[6] Failure to observe this NOE is not believed to be due to proton exchange since the observed line widths of the $^{AFB}G^4$ and G^{10} signals are comparable to the line widths of the other imino protons under these conditions. The corresponding NOE experiment could not be performed with d($AT^{AFB}GCAT)_2$ due to superposition of the imino resonances.

the major and minor groove of the modified oligodeoxynucleotide. Dipole–dipole interactions are observed between the aflatoxin H6a and H9a protons and major groove protons of the 5′-neighbor base. Thus, for d(ATC^{AFB}GAT)·d(ATCGAT) NOEs are observed between aflatoxin H6a and H9a and C^3 H5 and H6, whereas for d(AT^{AFB}GCAT)$_2$ the corresponding NOEs from aflatoxin H6a and H9a are observed to T^2 CH_3 and H6 (Tables III and IV; Figures 2 and 4). These NOEs demonstrate that aflatoxin H6a and H9a must be located in the major groove, and oriented in the 5′-direction from the site of modification. The aflatoxin methoxy and H5 protons show NOEs to the minor groove of the modified oligodeoxynucleotides. These NOEs are observed to deoxyribose H1′ and H4′ of ^{AFB}G and H1′ of its 5′-neighbor, which is C^3 in d(ATC^{AFB}GAT)·d(ATCGAT) and T^2 in d(AT^{AFB}GCAT)$_2$. Again, the pattern of NOEs suggests that the aflatoxin moiety must be oriented 5′ to the modified guanine residue. For d(AT^{AFB}GCAT)$_2$, an NOE is observed between 4-OCH_3 and A^5 H2, which provides strong evidence that the aflatoxin methoxy group is located in the minor groove of the modified oligodeoxynucleotide.[7] Only one NOE was observed between the aflatoxin moiety and a 3′-neighbor base pair to the site of adduction: between aflatoxin H8 and C^4 H5 in d(AT^{AFB}GCAT)$_2$. This NOE is consistent with intercalation of aflatoxin above the 5′-face of guanine, which would orient aflatoxin H8 in the major groove facing toward the 3′-neighbor base pair.

(3) Spin–lattice relaxation is consistent with an intercalated geometry in which the aflatoxin moiety interacts with both the minor and major grooves of d(ATC^{AFB}GAT)·d(ATCGAT) and d(AT^{AFB}GCAT)$_2$. The aflatoxin adduct produces an increased spin–lattice relaxation rate for adenine H2 protons. This observation suggests the proximity of aflatoxin protons to adenine H2 in the minor groove and is consistent with the observation of NOEs between A^5 H2 in d(AT^{AFB}GCAT)$_2$ and aflatoxin H3α and 4-OCH_3 protons (Table IV). Aflatoxin protons H8 and H9 also have substantially slower T_1 relaxation (Figure 7). In an intercalated geometry, aflatoxin protons H8 and H9 face into the major groove. The observation of only one NOE between aflatoxin H8 and the 3′-neighbor base pair in d(AT^{AFB}GCAT)$_2$ (Figure 2B; Table IV) suggests that these two aflatoxin protons are relatively isolated from spin–lattice relaxation pathways.

(4) Aflatoxin B_1 protons exhibit substantial upfield chemical shifts in d(ATC^{AFB}GAT)·d(ATCGAT) and d(AT^{AFB}GCAT)$_2$ as compared to free aflatoxins. The pattern of these chemical shift changes is comparable in both modified oligodeoxynucleotides. In both instances, the α protons at C2 and C3 show greater upfield shifts than do the β protons. Likewise, for both adducts, H5 shows a larger increased shielding while 4-OCH_3 shows a moderate increased shielding. In the major groove, the largest effect is observed for H9a in both cases. These observations suggest a similar orientation of the aflatoxin moiety in each of the two adducts. These chemical shift changes of as large as 1.0 ppm are consistent with the notion that the aflatoxin moiety is intercalated. They presumably arise from ring current effects due to stacking interactions. While the pattern of chemical shift changes is similar for the two adducts, the magnitudes of these perturbations differ in each case, probably due to nearest-neighbor influences at the site of adduction. The chemical shifts of the DNA protons are less disturbed by the presence of the adduct and are localized to the immediate vicinity of the modified base pair (Tables T5 and T6, supplementary material).

Assignment of the Aflatoxin Cyclopentenone Ring Protons. Determination of the orientation of the aflatoxin moiety allowed assignments of the aflatoxin cyclopentenone ring protons (Table I). If the aflatoxin is intercalated above the 5′-face of ^{AFB}G such that 4-OCH_3 and H5 face into the minor groove, then the cyclopentenone ring protons must also face into the minor groove such that H2α and H3α project toward the 5′-neighbor base pair, whereas H2β and H3β face the cytosine to which ^{AFB}G is base paired. In both modified oligodeoxynucleotides, a weak NOE was observed between cytosine H1′ of the C·^{AFB}G base pair and a cyclopentenone ring proton at C2, which was assigned as H2β. For d(AT^{AFB}GCAT)$_2$, a weak NOE was observed between A^5 H2 and a cyclopentenone ring proton at C3, which was assigned as H3α (panel B, Figure S5, supplementary material).

Reaction of Aflatoxin B_1 8,9-Epoxide with Duplex DNA. Adduct formation by aflatoxin B_1 is characterized by efficient regio- and stereoselectivity at guanine N7. No adducts other than 8,9-dihydro-8-(*N*7-guanyl)-9-hydroxyaflatoxin B_1 or the corresponding formamidopyrimidine (FAPY) rearrangement products have been identified (Essigmann et al., 1977; Lin et al., 1977; Baertschi et al., 1988). Conversion of aflatoxin B_1 8,9-epoxide to 8,9-dihydro-8-(*N*7-guanyl)-9-hydroxyaflatoxin B_1 with yields of as high as 80% is observed in the presence of 1.5 mM DNA (Baertschi et al., 1989). These observations are remarkable considering the hydrolytic instability of aflatoxin B_1 8,9-epoxide. In aqueous solution the half-life of the epoxide appears to be on the order of seconds due to formation of the corresponding dihydrodiol.[8] Aflatoxin B_1 has a relatively low affinity for DNA, with an association constant on the order of 10^3 (Stone et al., 1988; Gopalakrishnan et al., 1989b; Raney et al., 1990), and it is probable that aflatoxin B_1 8,9-epoxide has similar DNA binding affinity. These observations suggest that a specific orientation of bound epoxide facilitates formation of the transition state leading to guanine N7 adducts.

Loechler et al. (1988) argue that the structure of the transition state in the reaction between aflatoxin B_1 8,9-epoxide and guanine N7 and that of the resulting guanine N7 adduct are expected to be similar. This argument is based upon the rationale that, for the transition state in reactions involving oxocarbonium ions, bond formation is very incomplete whereas bond breaking is nearly complete (Koehler & Cordes, 1970; Cordes & Bull, 1974; Young & Jencks, 1977). Therefore, the transition state should be relatively insensitive to nucleophilic strength but quite sensitive to binding orientation. Consideration of the orientation of the available bonding orbital at guanine N7 suggests that intercalation of aflatoxin B_1 8,9-epoxide above the 5′-face of the reactive guanine provides excellent positioning for nucleophilic attack on the exo epoxide. The coumarin moiety and attached cyclopentenone ring of aflatoxin B_1 form a planar chromophore (Van Soest & Peerdeman, 1970) which can intercalate into DNA, as demonstrated by molecular modeling studies (Loechler et al., 1988; Bonnett & Taylor, 1989).

Evidence derived from binding studies using aflatoxins B_1 and B_2 as surrogates for the labile epoxide suggests that association of the epoxide with DNA is indeed intercalative (Stone et al., 1988; Gopalakrishnan et al., 1989b, Raney et al., 1990). When the effect of altering the cyclopentenone ring

[7] The corresponding NOE in d(ATC^{AFB}GAT)·d(ATCGAT) would occur between the exocyclic amino group of G^{10} and aflatoxin 4-OCH_3. That experiment was not performed.

[8] The hydrolysis rate for aflatoxin B_1 8,9-epoxide has not been quantitated. Qualitative measurements monitored by HPLC demonstrate complete conversion of the epoxide to the dihydrodiol within seconds.

Scheme I: Intercalation of the Aflatoxin Moiety above the 5′-Face of the Modified Guanine in d(ATC^{AFB}GAT)·d(ATCGAT) and d(AT^{AFB}GCAT)$_2$[a]

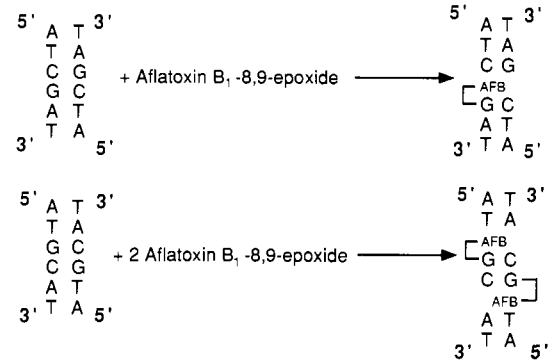

[a] The solution conformation as elucidated by NMR is consistent with the observed stoichiometry for reaction of aflatoxin B_1 8,9-epoxide with d(ATCGAT)$_2$ and d(ATGCAT)$_2$.

of aflatoxin B_1 to the less planar δ-lactone ring of aflatoxin G_1 (Cheung & Sim, 1964) was examined, the DNA association constant and the number of adducts formed at low DNA concentration were both decreased, which supports the hypothesis that the transition state for adduct formation involves an intercalated complex (Raney et al., 1990). Intercalation correctly orients aflatoxin B_1 8,9-epoxide for reaction at guanine N7 with the observed stereoselectivity, which probably accounts for the observed efficiency of adduct formation despite the relatively low DNA binding affinity.

Determination of conformation for d(ATC^{AFB}GAT)·d(ATCGAT) and d(AT^{AFB}GCAT)$_2$ does not provide direct information regarding the conformation of the transition state for the reaction between aflatoxin B_1 8,9-epoxide and DNA since rearrangement to the most thermodynamically stable conformation must occur following bond formation between guanine N7 and aflatoxin C8. Adduct conformation could differ from that of the transition-state complex, as has been proposed in the case of reaction between benzo[*a*]pyrene diol epoxide and guanine 2-NH_2 (Geacintov, 1985). However, comparison of chemical shift changes and spin–lattice relaxation rates for corresponding protons in either the associative complex or in these adducts suggests that the orientation of the aflatoxin moiety in d(ATC^{AFB}GAT)·d(ATCGAT) and d(AT^{AFB}GCAT)$_2$ is similar to that of aflatoxin B_1 in the corresponding noncovalent complexes (Gopalakrishnan et al., 1989a). A transition-state complex involving epoxide intercalation successfully predicts the stoichiometry of adduct formation which is observed for these two oligodeoxynucleotides (Scheme I). Insertion of aflatoxin B_1 8,9-epoxide above the 5′-face of a guanine in d(ATCGAT)$_2$, followed by formation of the N7 guanyl adduct, would prevent binding of a second molecule of aflatoxin B_1 8,9-epoxide. In contrast, two intercalation sites would be available for reaction with the sequence isomer d(ATGCAT)$_2$.

The results of the present NMR studies are not consistent with an alternative model advanced by Loechler and coworkers on the basis of molecular modeling studies, which proposes that both the transition state and the aflatoxin B_1 adduct are located in the major groove (Loechler et al., 1988). The NMR experiments demonstrate that the aflatoxin B_1 moiety interacts with both grooves of the modified oligodeoxynucleotide. The major groove model does not predict perturbation of minor groove protons such as adenine H2, which exhibits increased spin–lattice relaxation as well as dipolar coupling to aflatoxin H3α and 4-OCH_3. The characteristic B-DNA pattern of internucleotide NOEs between the base and deoxyribose protons and between the hydrogen-bonded imino protons would not be expected to be altered in both the modified and unmodified strands of the oligodeoxynucleotide were the aflatoxin moiety in the major groove. The substantially increased shielding of the aflatoxin protons is not consistent with the major groove model, which would predict instead some downfield shifts for aflatoxin protons. The difference in reaction stoichiometry for adduct formation with d(ATCGAT)$_2$ and d(ATGCAT)$_2$ is also difficult to reconcile with the major groove model, in which case one might expect that the reaction with d(ATCGAT)$_2$ could be forced to go beyond the observed stoichiometry of 1:1 aflatoxin B_1:d(ATCGAT)$_2$.

In summary, the present data lead to the conclusion that the aflatoxin moiety is intercalated in these modified oligodeoxynucleotides containing 8,9-dihydro-8-(*N*7-guanyl)-9-hydroxyaflatoxin B_1. A more precise understanding of the solution conformation for these adducts remains to be determined. Significant deformation of the double helix at the site of adduction may occur, resulting in bending or "hinging" of the helical axis at this location. The extent to which such deformation is present may play an important role in aflatoxin-induced mutagenesis. The tendency of these adducts to depurinate has hindered collection of quantitative NOE data for use in distance geometry (Nerdal et al., 1989) or restrained molecular dynamics calculations (Gronenborn & Clore, 1989). Calculational studies using molecular mechanics and molecular dynamics simulations have been initiated in an effort to develop a better understanding of adduct conformation.

Acknowledgments

We thank Professor Thomas R. Krugh and Suzanne Freeman O'Handley (The University of Rochester) for assistance in obtaining 500-MHz NOE data. The University of Rochester spectrometer was purchased in part with funding provided by shared Instrumentation Grants NIH RR03317 and NSF BBS-86-11927. We also thank Professor Edward L. Loechler (Boston University) for helpful discussions.

Supplementary Material Available

Six tables showing detailed ^1H NMR assignments, nonselective spin–lattice relaxation measurements, and chemical shift changes for d(ATC^{AFB}GAT)·d(ATCGAT) and d(AT^{AFB}GCAT)$_2$ and five figures showing HPLC chromatography, T_m analysis, strand mixing experiments as monitored by ^1H NMR, aflatoxin proton assignments, and sequential base–H2′,H2″ and H1′–H2′,H2″ assignments for d(ATC^{AFB}GAT)·d(ATCGAT) and d(AT^{AFB}GCAT)$_2$ (14 pages). Ordering information is given on any current masthead page.

Registry No. AFB_1 8,9-epoxide, 42583-46-0; d(ATCGAT), 84216-59-1; d(ATGCAT), 53263-13-1; d(AT^{AFB}GCAT), 122487-76-7.

References

Aoyama, T., Yamano, S., Guzelian, P. S., Gelboin, H. V., & Gonzalez, F. J. (1990) *Proc. Natl. Acad. Sci. U.S.A. 87*, 4790–4793.

Baertschi, S. W., Raney, K. D., Stone, M. P., & Harris, T. M. (1988) *J. Am. Chem. Soc. 110*, 7929–7931.

Baertschi, S. W., Raney, K. D., Shimada, T., Harris, T. M., & Guengerich, F. P. (1989) *Chem. Res. Toxicol. 2*, 114–122.

Bodenhausen, G., Kogler, H., & Ernst, R. R. (1984) *J. Magn. Reson. 58*, 370–388.

Bonnett, M., & Taylor, E. R. (1989) *J. Biomol. Struct. Dyn. 7*, 127–149.
Busby, W. F., Jr., & Wogan, G. N. (1984) in *Chemical Carcinogens* (Searle, C., Ed.) 2nd ed., ACS Monograph 182, pp 945–1136, American Chemical Society, Washington, DC.
Cheung, K. K., & Sim, G. A. (1964) *Nature (London) 201*, 1185–1188.
Cordes, E. H., & Bull, H. G. (1974) *Chem. Rev. 74*, 581–603.
Croy, R. G., Essigmann, J. M., Reinhold, V. M., & Wogan, G. N. (1978) *Proc. Natl. Acad. Sci. U.S.A. 75*, 1745–1749.
Essigmann, J. M., Croy, R. G., Nadzan, A. M., Busby, W. F., Jr., Reinhold, V. N., Büchi, G., & Wogan, G. N. (1977) *Proc. Natl. Acad. Sci. U.S.A. 74*, 1870–1874.
Essigmann, J. M., Green, C. L., Croy, R. G., Fowler, K. W., Büchi, G., & Wogan, G. N. (1983) *Cold Spring Harbor Symp. Quant. Biol. 47*, 327–337.
Feigon, J., Denny, W. A., Leupin, W., & Kearns, D. R. (1983) *Biochemistry 22*, 5943–5951.
Garner, R. C. (1980) *Br. Med. Bull. 36*, 47–52.
Garner, R. C., Miller, E. C., & Miller, J. A. (1972) *Cancer Res. 32*, 2058–2066.
Geacintov, N. E. (1985) in *Polycyclic Hydrocarbons and Carcinogenesis* (Harvey, R. G., Ed.) ACS Monograph 283, pp 107–124, American Chemical Society, Washington, DC.
Gopalakrishnan, S., Stone, M. P., & Harris, T. M. (1989a) *J. Am. Chem. Soc. 111*, 7232–7239.
Gopalakrishnan, S., Byrd, S., Stone, M. P., & Harris, T. M. (1989b) *Biochemistry 28*, 726–734.
Gronenborn, A. M., & Clore, G. M. (1989) *Biochemistry 28*, 5978–5984.
Hare, D. R., Wemmer, D. E., Chou, S. H., Drobny, G., & Reid, B. R. (1983) *J. Mol. Biol. 171*, 319–336.
Hilbers, C. W., & Patel, D. J. (1975) *Biochemistry 14*, 2656–2660.
Hore, P. J. (1983a) *J. Magn. Reson. 54*, 539–542.
Hore, P. J. (1983b) *J. Magn. Reson. 55*, 283–300.
Hsieh, D. P. H., & Wong, J. J. (1982) in *Biological Reactive Intermediates* (Snyder, R., et al., Eds.) pp 847–863, Plenum Press, New York.
Israel-Kalinsky, H., Tuch, J., Roitelaman, J., & Stark, A.-A. (1982) *Carcinogenesis (London) 3*, 423–429.
Koehler, K., & Cordes, E. H. (1970) *J. Am. Chem. Soc. 92*, 1576–1582.
Krugh, T. R., Graves, D. E., & Stone, M. P. (1989) *Biochemistry 28*, 9988–9994.
Lin, J. K., Miller, J. A., & Miller, E. C. (1977) *Cancer Res. 37*, 4430–4438.
Loechler, E. L., Teeter, M. M., & Whitlow, M. D. (1988) *J. Biomol. Struct. Dyn. 5*, 1237–1257.
McCann, J., Springarn, N. E., Kobori, J., & Ames, B. N. (1975) *Proc. Natl. Acad. Sci. U.S.A. 72*, 979–983.
Misra, R. P., Muench, K. F., & Humayun, M. Z. (1983) *Biochemistry 22*, 3351–3359.
Mori, H., Sugie, S., Yoshimi, N., Kitamura, J., Niwa, M., Hamasaki, T., & Kawai, K. (1986) *Mutat. Res. 173*, 217–222.
Nerdal, W., Hare, D. R., & Reid, B. R. (1989) *Biochemistry 28*, 10008–10021.
Oda, Y., Nakamura, S., Oki, I., Kato, T., & Shinagawa, H. (1985) *Mutat. Res. 147*, 219–229.
Patel, D. J. (1974) *Biochemistry 13*, 2396–2402.
Plateu, P., & Gueron, M. (1982) *J. Am. Chem. Soc. 104*, 7310–7311.
Raney, K. D., Gopalakrishnan, S., Byrd, S., Stone, M. P., & Harris, T. M. (1990) *Chem. Res. Toxicol. 3*, 254–261.
Shaulsky, G., Johnson, R. L., Shockcor, J. P., Taylor, L. C. E., & Stark, A.-A. (1990) *Carcinogenesis 11*, 519–527.
Shimada, T, & Guengerich, F. P. (1989) *Proc. Natl. Acad. Sci. U.S.A. 86*, 462–465.
Shimada, T., Nakamura, S.-I., Imaoka, S., & Funae, Y. (1987) *Toxicol. Appl. Pharmacol. 91*, 13–21.
Sklenar, V., & Bax, A. (1987) *J. Magn. Reson. 74*, 469–479.
Sklenar, V., Brooks, B. R., Zon, G., & Bax, A. (1987) *FEBS Lett. 216*, 249–252.
Stark, A.-A., Gal, Y., & Shaulsky, G. (1990) *Carcinoge[illegible]s 11*, 529–534.
Stone, M. P., Gopalakrishnan, S., Harris, T. M., & Gra[illegible], D. E. (1988) *J. Biomol. Struct. Dyn. 5*, 1025–1041.
Van Soest, T. C., & Peerdeman, A. F. (1970) *Acta Crystallogr. B26*, 1940–1955.
Wong, J. J., Singh, R., & Hsieh, D. P. H. (1977) *Mutat. Res. 44*, 447–450.
Young, P. R., & Jencks, W. P. (1977) *J. Am. Chem. Soc. 99*, 8238–8248.
Yourtee, D. M., Kirk-Yourtee, C. L., & Searles, S. (1987) *Life Sci. 41*, 1795–1803.